A Global Reassessment of the Spatial and Temporal Expression of the Late Miocene Biogenic Bloom

Q. Pillot, B. Suchéras-Marx, A.-C. Sarr, C. Bolton, Y. Donnadieu

Paleoceanography and Paleoclimatology

AGU ADVANCING EARTH AND SPACE SCIENCE

RESEARCH ARTICLE
10.1029/2022PA004564

Key Points:

- The Late Miocene Biogenic Bloom (LMBB) is expressed in sediment cores in various oceanographic settings
- Almost 40% of the sites in the compilation show no expression of the LMBB signal
- The onset of the LMBB could be linked to a generalized increase in upwelling activity

Supporting Information:

Supporting Information may be found in the online version of this article.

Correspondence to:

Q. Pillot and B. Suchéras-Marx,
pillot@cerege.fr;
sucheras-marx@cerege.fr

Citation:

Pillot, Q., Suchéras-Marx, B., Sarr, A.-C., Bolton, C. T., & Donnadieu, Y. (2023). A global reassessment of the spatial and temporal expression of the Late Miocene Biogenic Bloom. *Paleoceanography and Paleoclimatology*, *38*, e2022PA004564. https://doi.org/10.1029/2022PA004564

Received 10 OCT 2022
Accepted 8 MAR 2023

Author Contributions:

Conceptualization: Q. Pillot, B. Suchéras-Marx
Data curation: Q. Pillot
Formal analysis: Q. Pillot, B. Suchéras-Marx
Funding acquisition: B. Suchéras-Marx
Investigation: Q. Pillot, B. Suchéras-Marx, A.-C. Sarr, C. T. Bolton, Y. Donnadieu
Methodology: Q. Pillot, B. Suchéras-Marx
Project Administration: Y. Donnadieu
Software: Q. Pillot
Supervision: B. Suchéras-Marx

A Global Reassessment of the Spatial and Temporal Expression of the Late Miocene Biogenic Bloom

Q. Pillot[1], B. Suchéras-Marx[1], A.-C. Sarr[1], C. T. Bolton[1], and Y. Donnadieu[1]

[1]Aix Marseille Univ, CNRS, IRD, INRAE, CEREGE, Aix-en-Provence, France

Abstract The Late Miocene Biogenic Bloom (LMBB) is a late Miocene to early Pliocene oceanographic event characterized by high accumulation rates of opal from diatoms and calcite from calcareous nannofossils and planktic foraminifera. This multi-million year event has been recognized in sediment cores from the Pacific, Atlantic, and Indian Oceans. Based on existing studies, it is not clear whether the LMBB is a global omnipresent event, or whether it is restricted to certain regions or oceanographic environments. Moreover, the origin of this event is still widely discussed. In this study, we aim to provide a comprehensive overview of the geographical and temporal aspects of the LMBB by compiling published ocean drilling (DSDP, ODP, and IODP) records of sedimentation rates, and $CaCO_3$, opal, and terrigenous accumulation rates that cover the late Miocene and early Pliocene interval. Our data compilation shows that manifestations of the LMBB are present in many different locations but in a very heterogeneous way. The compilation shows that the sites where the LMBB is expressed are mainly located in areas with a high productivity regime (i.e., upwelling systems). We suggest that one of the possible hypotheses to explain the onset of the LMBB could be a global increase in upwelling intensity due to an increase in wind strength or an increase in deep water formation, ramping up global thermohaline circulation.

1. Introduction

The late Miocene and the early Pliocene are marked by a major event recognized in deep-sea sediments called the Late Miocene Biogenic Bloom (LMBB). This event is characterized by high rates of opal accumulation from diatoms and radiolarians and high rates of calcite accumulation from calcareous nannofossils and planktonic foraminifera (e.g., Bolton et al., 2022; Dickens & Owen, 1999; Diester-Haass et al., 2005; Drury et al., 2021; Farrell et al., 1995; Grant & Dickens, 2002; Lyle & Baldauf, 2015). A comprehensive review of the temporal and geographical aspects of the LMBB would help to better understand the causes of this event and its impact on the carbon cycle. The LMBB event, first described by Farrell et al. (1995), has been recovered in multiple sites of the world ocean (Figure 1), but its timing is heterogeneous across the sites and its signature in the data record has been identified from a variety of different proxies. Farrell et al. (1995) define the LMBB based on an increase in biogenic deposits ($CaCO_3$, biogenic silica [opal], and nannofossils) between 6.7 and 4.5 million years ago (Ma) in the Eastern Equatorial Pacific Ocean, and interpret this increase to be related to increased biological productivity. The Eastern Equatorial Pacific region was also studied by Lyle and Baldauf (2015) who observed the LMBB between 8 and 4.5 Ma, marked by long periods of high opal and $CaCO_3$ deposition. Records from the same region, with better resolution and updated age models, were used by Lyle et al. (2019) to estimate the end of the event at about 4.4 Ma, at a time of major decrease in sedimentation rate. Outside of the East Equatorial Pacific, Grant and Dickens (2002) identified the LMBB event in the southwestern Pacific Ocean, where it takes the form of an increase in $CaCO_3$ mass accumulation between 9 and 3.8 Ma with a maximum around 5 Ma. L. Zhang et al. (2009) identified the LMBB in records from the South China Sea that exhibit increased mass accumulation of $CaCO_3$ and opal between 12 and 6 Ma. In the Atlantic Ocean, Diester-Haass et al. (2005) identified the LMBB in three different regions. In the North Atlantic, $CaCO_3$ mass accumulation rate (MAR) and benthic foraminiferal accumulation rates reached a maximum at 5 Ma. This maximum was observed earlier in records from the tropical ocean (around 6 Ma) and the South Atlantic Ocean (around 8.2 Ma). In the South Atlantic (ODP site 208-1264), Drury et al. (2021) studied the evolution of $CaCO_3$ MAR at orbital resolution. The onset of the LMBB is detected at 7.8 Ma and the end at 3.3 Ma with an optimum between 7 and 6.4 Ma. Records from lower productivity regions in the Atlantic and Indian Oceans have also been used to identify the LMBB (Hermoyian & Owen, 2001). By measuring the rate of mass accumulation of phosphorus, they found a signature of the LMBB with peak productivity around 4–5 Ma. In the Indian Ocean, an increase in productivity between 9 and 3.5 Ma

Validation: Q. Pillot, B. Suchéras-Marx, Y. Donnadieu
Writing – original draft: Q. Pillot, B. Suchéras-Marx, A.-C. Sarr, C. T. Bolton, Y. Donnadieu
Writing – review & editing: Q. Pillot, B. Suchéras-Marx, A.-C. Sarr, C. T. Bolton, Y. Donnadieu

was identified by Dickens and Owen (1999) which is reflected in an increase in $CaCO_3$ mass accumulation as well as the spatial expansion of the Oxygen Minimum Zone. Nevertheless, Lübbers et al. (2019) suggest a much earlier onset of the LMBB in the Indian Ocean at 11.2 Ma based on an increase in Log (Ba/Ti) associated with a change in sediment color from red to green.

This increase in biogenic sedimentation is coeval with significant changes in the global climate system. Although the land-sea distribution has been quasi-stable since the late Miocene, the configuration of several major seaways evolved during this period: the Central American Seaway underwent restriction (O'Dea et al., 2016), the Bering Seaway opened (Gladenkov & Gladenkov, 2004), and the Indonesian Seaway underwent progressive restriction (Kuhnt et al., 2004), all of which likely triggered major changes in oceanic circulation (e.g., Brierley & Fedorov, 2016). Alongside these paleogeographic changes, global cooling occurred at the end of the Miocene, associated with an increase in the meridional sea surface temperature gradient (Herbert et al., 2016; Martinot et al., 2022). The global decrease in temperature is probably driven by a significant drop in the partial pressure of CO_2 in the atmosphere (pCO_2) from about 600 ppm in the middle Miocene to about 400 ppm in the early Pliocene (e.g., Rae et al., 2021). The establishment of a small permanent ice on Greenland is also inferred during the late Miocene (Bierman et al., 2016; Helland & Holmes, 1997; John & Krissek, 2002). The expansion of deserts may also be contemporary with this period (Schuster et al., 2006; Z. Zhang et al., 2014), although recent data from the tropical Atlantic margin highlight that the Sahara desert already existed 11 Ma ago (Crocker et al., 2022). Vegetation on land also underwent significant changes with the rise to dominance of plants using C_4 photosynthesis at the detriment of plants using C_3 photosynthesis (Cerling et al., 1997; Tauxe & Feakins, 2020). Some of these changes have been suggested as possible triggering mechanisms for the LMBB.

Two hypotheses, not incompatible with each other, have been proposed to explain the origin of the LMBB. This event could result from (a) an increase in nutrient supply from the continents to the oceans (e.g., Filippelli, 1997; Gupta et al., 2004; Hermoyian & Owen, 2001; Pisias et al., 1995) or (b) a redistribution of nutrients in the ocean due to a reorganization of oceanic circulation (e.g., Dickens & Owen, 1999; Farrell et al., 1995; Pisias et al., 1995).

An increase in nutrient supply is usually attributed either to enhanced weathering or to a shift in vegetation cover. A late uplift pulse in the Tibetan Plateau region (C. Wang et al., 2014) could have been responsible for intensification of the Indian monsoon and the increase in continental weathering during the late Miocene (Clift et al., 2020; Filippelli, 1997; Holbourn et al., 2018; Yang et al., 2019). This hypothesis is supported by the global increase in Ca and Si fluxes to the ocean (Pisias et al., 1995). Hermoyian and Owen (2001) also suggest that the uplift of the Andes at 8 Ma caused orographic precipitation and increased sediment flux to the Atlantic Ocean (Curry et al., 1995). An increase in nutrient supply from the continents could also be explained by an intensification of trade winds at the end of the Miocene, associated with the increase in latitudinal temperature gradient as well as a widespread continental aridification (Diester-Haass et al., 2006; Dobson et al., 2001; Herbert et al., 2016; Hovan, 1995). A further hypothesis also suggests that the global spread of C_4 plants in the late Miocene would have resulted in the input of siliceous phytoliths into the ocean reservoir and may have played a role in increasing productivity by reducing silica limitation (Cortese et al., 2004; Pound et al., 2012).

The alternative hypothesis is the redistribution of nutrients caused by changes in oceanic circulation. Based on microfossil and $\delta^{13}C$ studies, Berger et al. (1993) suggested that an amplification of North Atlantic Deep Water (NADW; Wright & Miller, 1996) brought more nutrients into the Pacific Ocean, although Farrell et al. (1995) rather suggest no temporal link between NADW evolution and the LMBB. The restriction of the Central American Seaway may have played a role in the redistribution of nutrients by changing oceanic circulation patterns (Farrell et al., 1995; Pisias et al., 1995). Diester-Haass et al. (2002) also suggest that a change in the vertical distribution of nutrients could result from an intensification of the global ocean circulation forced by an intensification of trade winds or by an increase in latitudinal temperature gradient (caused by the global decrease in pCO_2 and the growth of polar ice sheets).

While the initiation of the LMBB has been widely discussed in the literature (e.g., Dickens & Owen, 1999; Diester-Haass et al., 2002, 2006; Farrell et al., 1995; Reghellin et al., 2022), the termination of the event has been the subject of only a limited number of studies. Farrell et al. (1995) observe a distinct and permanent shift in the location of the maximum opal MAR at 4.4 Ma synchronous with the end of the LMBB. The authors attribute this shift to the final closure of the Central American Seaway that prevented surface water from being exchanged between the Atlantic and Pacific Oceans. More recently, Karatsolis et al. (2022) link the end of the LMBB with

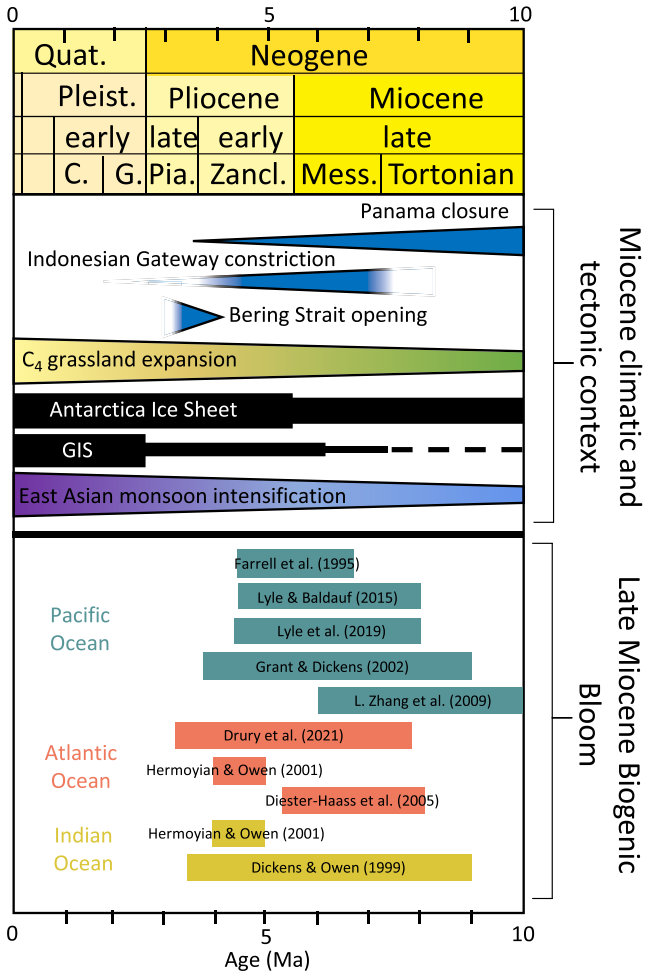

Figure 1. At the top, figure adapted from Steinthorsdottir et al. (2021). Evolution of major seaways configuration during the late Miocene and Pliocene (Gladenkov & Gladenkov, 2004; Kuhnt et al., 2004; O'Dea et al., 2016), C_4 grassland expansion (Tauxe & Feakins, 2020), Antarctica and Greenland Ice sheet (GIS) evolution (Bierman et al., 2016; Cook et al., 2013), and East Asian monsoon intensification (Holbourn et al., 2018). Bottom, compilation of some publications related to the LMBB. Stages acronyms: Mess. (Messinian), Zancl. (Zanclean), Pia. (Piacenzian), G. (Gelasian), and C. (Calabrian).

a decrease in insolation due to a particular orbital configuration. This drop in insolation would have caused a reduction in hydrological cycle intensity and therefore a decrease in continental weathering and nutrient supply to the ocean.

Because most published work on the LMBB focuses on specific cores where the event is recorded, we know where the bloom is present but not where it is potentially not expressed. A global overview of the event is therefore lacking. We therefore systematically compiled all available/published paleoceanographic records (from Deep Sea Drilling Project [DSDP], Oceanic Drilling Program [ODP], Integrated Ocean Drilling Program [IODP], and International Ocean Discovery Program [IODP]), that inform on sediment accumulation during the late Miocene to early Pliocene time period. This compilation contains records of sedimentation rates as well as accumulation rates of $CaCO_3$, opal, and terrigenous material and provides a thorough analysis of the spatial and temporal distribution of the LMBB.

2. Methods

We compiled oceanographic data from DSDP, ODP, and IODP expeditions that cover the late Miocene and early Pliocene. Data mining was performed by automatically collecting the Pangaea data sets that correspond to the selected time interval and that have at least one of the following variables: sedimentation rate, dry bulk density, MAR, $CaCO_3$ accumulation rate, $bSiO_2$ accumulation rate (biogenic SiO_2), $\%CaCO_3$, $\%bSiO_2$. The compilation was then improved by manually adding data sets absent from Pangaea but relevant to our study. The data compilation contains 154 data sets (122 are from Pangaea) from 118 different ocean drilling sites (Table 1). We assumed that in each publication, one site represents one data set, which means that in a publication there are as many sites as data sets. There can therefore be several data sets per publication but also several data sets per site if several publications have studied the site in question. In contrast to Karatsolis et al. (2022) who choose to focus on high-resolution records only, we here choose a less selective approach because even lower resolution data sets or data sets that show no signature of the LMBB can help us understand its origin.

The data sets were manually labeled by two different person to indicate whether they contained the LMBB signature. The LMBB signature is defined as an increase (in carbonate or biogenic opal MAR or sedimentation rate) followed by a decrease to a pre-event level and occurring during the late Miocene to early Pliocene (Dickens & Owen, 1999). The results are split into four categories as follows: (a) "No," if the data set shows no LMBB signature; (b) "BB," if the LMBB is clearly identifiable; (c) "Co," if the occurrence of the LMBB is controversial, that is, in case an increase in biogenic production can be identified but the timing is not consistent with the LMBB definition. This label is also used for data sets that show potential traces of the LMBB but that could be classified as "BB" or "No" depending on the person performing the evaluation; (d) "In," if there are not enough data before or after the interval of interest to robustly identify an increase followed by a decrease ("In" standing for "inconclusive," Figure S4 in Supporting Information S1). In the latter case, we cannot conclude whether the LMBB is present in the data set. The variables used to define the label are detailed for each data set in Table S1. Sites were also labeled according to the labels of the associated data sets. In cases where there were multiple data sets for a single site, the label was assigned based on all data sets considered together; in case there was a contradiction between data set labels, the label of the data set with the highest temporal resolution was chosen. The interpretations and conclusions of the original publications have not been taken into account to keep a homogeneity in the labeling criteria.

As the data sets have age-depth models calibrated on different time scales (Berggren et al., 1985, 1995; Gradstein et al., 2004, 2012, 2020; Palike et al., 2006), we re-calibrated every single age-depth model to the Gradstein

Table 1
Source of the Data Used for the Compilation

Publication	Number of data sets	Variables present in these data sets
Breza (1992)	1	Sed rate
Diester-Haass et al. (2004)	2	Acc rate $CaCO_3$
Diester-Haass et al. (2005)	3	Sed rate, Acc rate $CaCO_3$, $CaCO_3$, DBD
Diester-Haass et al. (2006)	4	Sed rate, MAR, Acc rate $CaCO_3$, $CaCO_3$
Drury et al. (2021)	1	Sed rate, $CaCO_3$, Acc rate $CaCO_3$, MAR, DBD
Dutkiewicz and Müller (2021)	16	Acc rate $CaCO_3$, DBD, $CaCO_3$, Sed rate
Farrell and Janecek (1991)	1	Sed rate, Acc rate $CaCO_3$, $CaCO_3$, DBD
Farrell et al. (1995)	11	Sed rate, Acc rate $CaCO_3$, $CaCO_3$, DBD
Gardner et al. (1986)	2	Sed rate, MAR, Acc rate $CaCO_3$, $CaCO_3$
Grant and Dickens (2002)	1	Acc rate $CaCO_3$, $CaCO_3$
Hayward et al. (2010)	1	Sed rate
Hermoyian and Owen (2001)	5	Sed rate, DBD
Janecek (1985)	2	Sed rate, MAR, DBD
Lyle et al. (1995)	11	Sed rate, Acc rate $CaCO_3$, $CaCO_3$
Lyle (2003)	57	Sed rate, MAR, Acc rate $CaCO_3$, $CaCO_3$, DBD
Lyle et al. (2019)	7	Sed rate, MAR, $CaCO_3$, DBD, $bSiO_2$
D. W. Müller et al. (1991)	1	Sed rate, MAR, Acc rate $CaCO_3$, DBD
Pälike et al. (2012)	4	Sed rate, MAR, $CaCO_3$, DBD, Acc rate $CaCO_3$
Peterson and Backman (1990)	3	MAR, Acc rate $CaCO_3$, $CaCO_3$
Si and Rosenthal (2019)	13	$CaCO_3$, MAR, Acc rate $CaCO_3$, Sed rate
Stax and Stein (1993)	4	MAR
Wagner (2002)	1	Sed rate, MAR
R. Wang et al. (2004)	1	Acc rate opal, $bSiO_2$
Winkler (1999)	1	Sed rate, MAR, Acc rate $CaCO_3$, $CaCO_3$
L. Zhang et al. (2009)	1	Sed rate, MAR, DBD

Note. Sed rate: Sedimentation rate. Acc rate: Accumulation rate. MAR: Mass Accumulation Rate. DBD: Dry Bulk Density. A more detailed table can be found in Table S1.

et al. (2020) time scale to be able to perform a temporal comparison of the data sets. This step was performed using the Neptune Sandbox Berlin database (Renaudie et al., 2020) and NSB Companion software (Renaudie, 2019), following a procedure similar to the one in Dutkiewicz and Müller (2022).

In addition, a geographical and temporal averaging system was implemented to plot time series. For a given oceanic basin (Pacific, Atlantic, and Indian) and a given variable, all values of the corresponding data sets were grouped and segmented into 500 kyr bins to obtain a single time series. This segmentation implies that the values of the bins are dated at ±250 kyr. 500 kyr was chosen because many data sets—in particular Lyle (2003)—had a resolution of 500 kyr. In each bin, data were averaged in two different ways: (a) The "same weight" average where each data set is averaged individually before being averaged together. With this method, each data set will have the same weight in a bin, regardless of its resolution; (b) The "resolution weight" average where data sets are directly averaged together. With this average, the more data a data set contains in a given bin, the more weight it will have in determining the final average value.

We then tried to identify potential oceanographic similarities between sites where the LMBB is present or absent. To do so, we used information from an ocean biogeochemical simulation for the late Miocene from Sarr et al. (2022). This simulation using late Miocene/early Pliocene paleogeography was performed with the IPSL-CM5A2 Earth System model (Sepulchre et al., 2020) coupled with the PISCES-v2 model (Aumont

et al., 2015). PISCES-v2 is a biogeochemical model that simulates marine ecosystems (including diatoms, nanophytoplankton, microzooplankton, and mesozooplankton) and major biogeochemical cycles. We here used the organic productivity by phytoplankton. Organic productivity is a good indicator of the area of higher productivity from calcareous and siliceous phytoplankton and zooplankton. In this model, phytoplankton growth is limited by the availability of nutrients (phosphorus, nitrogen, iron, and silica), by light, and by water temperature (see Aumont et al., 2015, for detailed equations). To superimpose the position of the sites on the simulation outputs, we recalculated the paleocoordinates of each site at 10 Ma using the GPlates software (Qin et al., 2012) and the plate rotation model from R. D. Müller et al. (2019), Cao et al. (2022), and Young et al. (2019) with the Torsvik et al. (2019) correction applied for the Pacific. In the following, the paleocoordinates will only be used for comparison with model outputs.

A table with the following information for each data set is available in Table S1 and on SEANOE (Pillot, 2023): site number, data set label, site label, publication, elevation, site coordinates, site paleocoordinates (10 Ma), available variables, variables used for labeling, the time scale used in the original publication, and the web link to the original data set.

3. Results

3.1. Geographical Analysis of the Compilation

Among the 118 sites, the LMBB is present at 21 sites (BB), while 33 other sites remain controversial (Co). The LMBB is not present in 45 of the sites (No) and its presence is inconclusive for 19 of the sites (In). The LMBB is identified in both the Pacific, Atlantic, and Indian Oceans (sites labeled "BB" and "Co," Figure 2). Most of the sites with an LMBB are localized at mid and low latitudes, suggesting that the LMBB is either absent or has not been recovered in the Southern or in Arctic Oceans. The LMBB has been identified (certainly or controversially) in all the sites from the northern part of the Indian Ocean. The presence of the LMBB in the Pacific and Atlantic Oceans is very heterogeneous. In some areas, sites with an LMBB signature and without an LMBB signature are very close geographically, such as in the Eastern Equatorial Pacific (i.e., DSDP site 85-572 and ODP site 138-850 or ODP sites 138-852 and 138-853). The controversial sites have a more homogeneous distribution in terms of latitude.

The spatial distribution of sites where the LMBB has been clearly identified follows the same pattern as those where the presence of LMBB is controversial. There are only three sites that show a clear LMBB signature in the Atlantic basin, one in the Indian basin and all the remaining ones are located in the Pacific basin. Most of the LMBB sites are located in the low latitudes (between 30°S and 30°N; Figures 2a, 3d and 3e), except for ODP site 145-883 which is located in the northern Pacific.

In the Atlantic Ocean, areas where LMBB is clearly identifiable (off the American coastlines at 5°N–40°E and off the African coastlines at 30°S–4°W) are also areas where there are sites with no LMBB evidenced. Most of the isolated sites are sites without an LMBB signature and are located around the Mid-Atlantic Ridge. There is, however, a controversial presence of the LMBB at three isolated and open-ocean sites (ODP site 162-982, ODP site 177-1088, and DSDP site 73-519).

In the Pacific Ocean, the LMBB signature is present off the coast of Australia, in the northern area of the Tasman Sea and also in the northern part of the Pacific Ocean. The LMBB is also mainly present in the eastern equatorial part, although there are also many sites without signature of the LMBB in this area. The Eastern Equatorial Pacific has a high concentration of sites with many of them showing the presence of the LMBB. Sites with an LMBB signature are mainly located between 5°N and 5°S, while the sites without an LMBB signature are a few degrees further north and further south (except for DSDP site 85-572).

In the Indian Ocean, the presence of the LMBB is in most cases controversial but one site clearly records it in the western tropical area, near the Seychelles archipelago (ODP site 115-707). In the southern Indian Ocean, the compilation has only two sites and they do not show any evidence of the LMBB. The remaining sites do not have enough data to conclude.

3.2. Statistical Analysis of Compilation

The present-day water depth of the sites where the LMBB is absent ranges between 1,000 and 5,000 m with a large proportion of sites around 3,500 m (Figure 3f). The depth of the sites where the LMBB is present is mainly

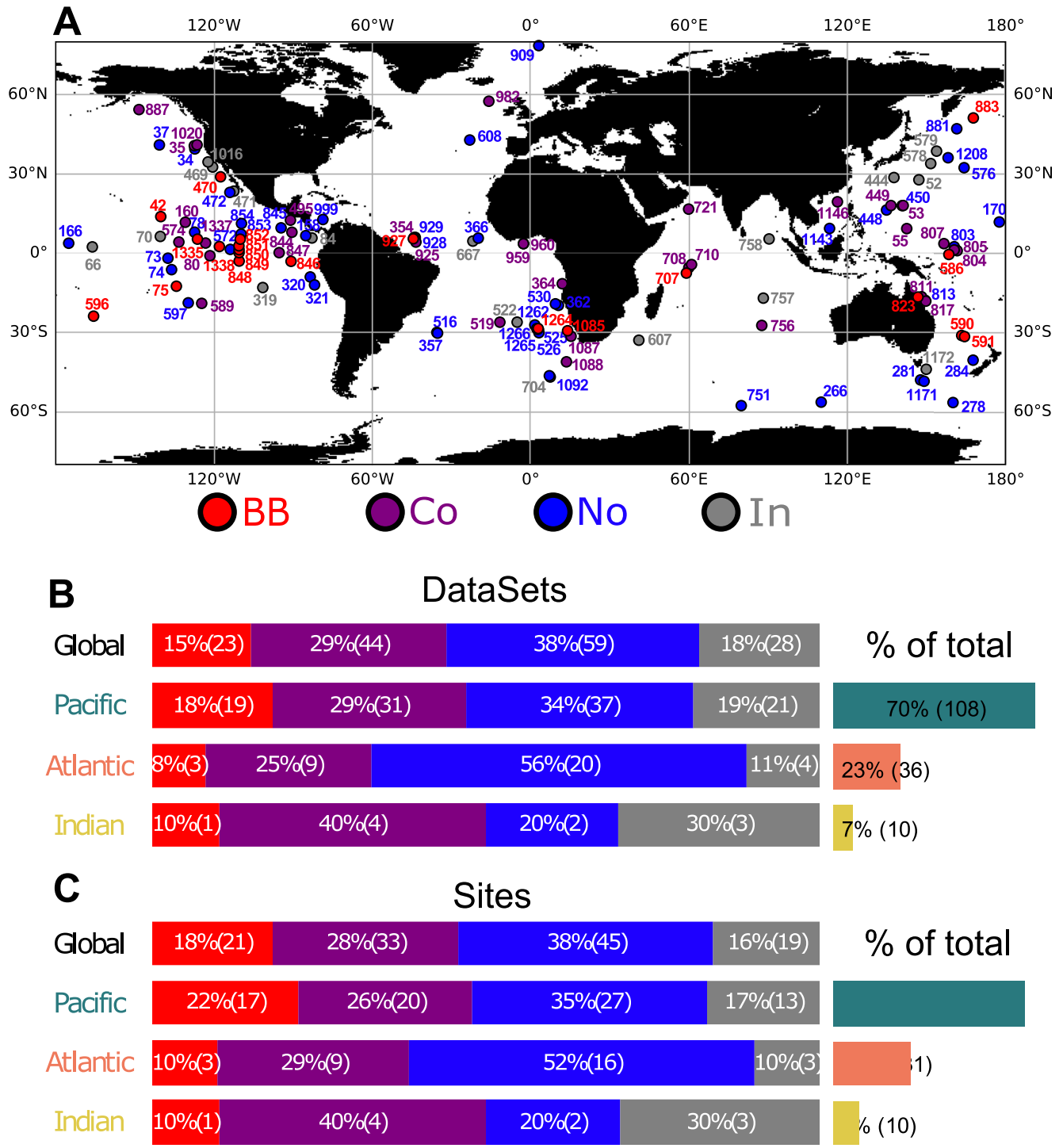

Figure 2. (a) Present-day coastlines with dots showing the modern positions of the 118 labeled sites. (b) Distribution of labels for the 154 data sets, with the absolute value in brackets. (c) Distribution of labels for the 118 sites, with the absolute value in brackets. "In"—Inconclusive; "No"—No LMBB; "Co"—Controversial LMBB; and "BB"—LMBB is present.

between 1,500 and 4,000 m. The average depth of sites where the LMBB is present (3,236 m) is almost equal to that of sites where the LMBB is absent (3,225 m). This suggests that, on a global scale, the geographic distribution of sites where the LMBB is unambiguously identified may not be biased by site depth. Though we are aware that bathymetry has likely evolved since the late Miocene, we think that using the drilling elevation is more meaningful at global scale than using paleobathymetry reconstruction, which has a poor resolution. We note that

10.1029/2022PA004564

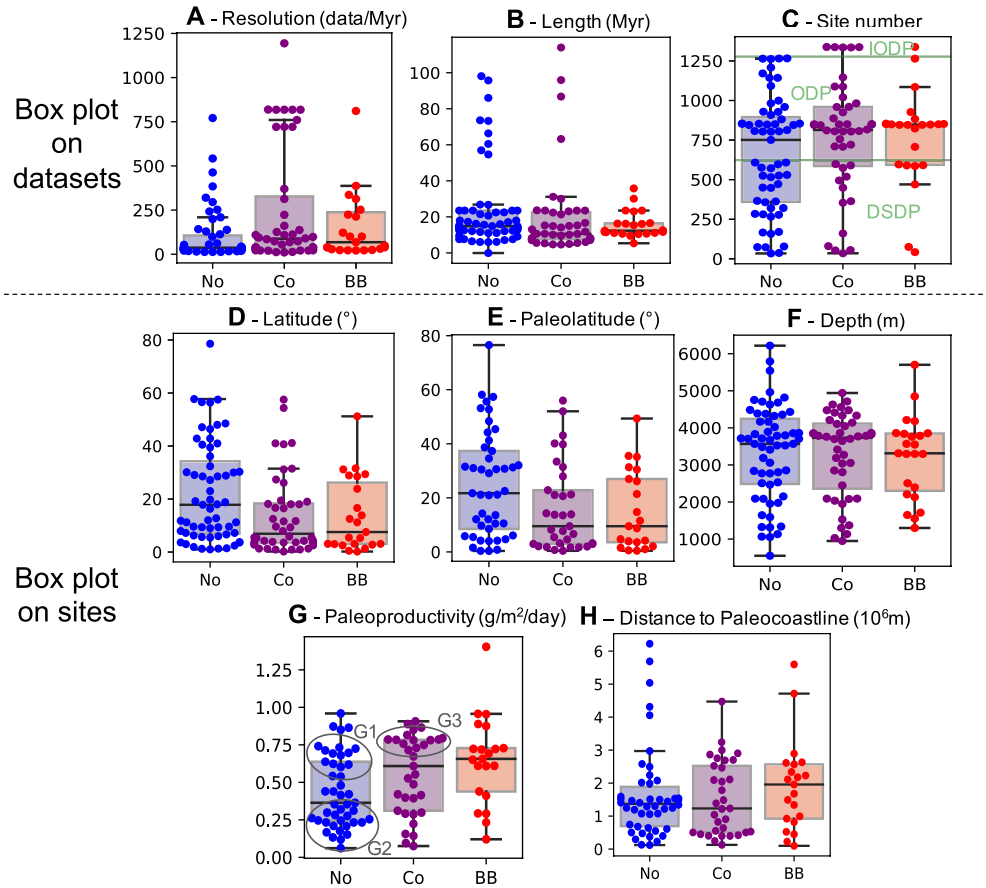

Figure 3. (a–c) Box plot calculated on the data sets (each point represents a data set). (d–i) Box plot calculated on the sites (each point represents a site). "No"— No LMBB; "Co"— Controversial LMBB; and "BB"—LMBB is present. (a) Data set resolution in number of data per million years. The data set from Drury et al. (2021) is not shown because it is out of range (24,800 data/Myr). (b) Signal length (Myr). (c) Site numbers with program names. (d) Absolute modern latitude values in degrees. (e) Absolute paleolatitude (10 Ma) values in degrees. (f) Depth of sites in meters. (g) Integrated primary productivity value by phytoplankton from a late Miocene simulation in g/m^2/day (from Sarr et al., 2022) retrieved with the paleocoordinates. (h) Distance between the paleocoordinates of the sites and the nearest coast in the late Miocene simulation (m).

at some particular places, where the bathymetric feature has a likely young vertical deformation history, it might bias the interpretation.

The simulated paleoproductivity at sites where an LMBB signature is visible is 0.66 g/m^2/day on average (Figure 3g). Although most of the sites are located in areas of high simulated palaeoproductivity (>0.7 g/m^2/day—e.g., East Equatorial Pacific and Southeast Atlantic Ocean), the LMBB is also identified in some oligotrophic areas (<0.3 g/m^2/day—e.g., North Pacific, South Pacific Gyre; Figure S3 in Supporting Information S1). For sites where the LMBB is absent, the average simulated palaeoproductivity is 0.48 g/m^2/day. However, two groups can be distinguished, one around 0.25 g/m^2/day and one around 0.75 g/m^2/day (Figure 3g, G1 and G2). A group around 0.75 g/m^2/day also emerged in controversial sites (Figure 3g, G3).

To estimate the possible impact of continental nutrient inputs, the distance between each site paleolocation and the nearest paleocoastline was calculated (Figure 3h). Most of the sites with no LMBB signature were located less than 2,000 km from the nearest coastline (on average 1,650 km) with fivvve sites at more than 4,000 km. In contrast, most of the sites labeled "BB" were located between 100 and 3,000 km from the nearest coastline (on average 1,922 km). Concerning the distances to the nearest coastline of the sites labeled "Co," the distribution is as wide as for the sites labeled "BB," ranging from 100 to 3,000 km away from the nearest coastline (on average 1,543 km). A map with the plotted distances is available in Figure S5 in Supporting Information S1.

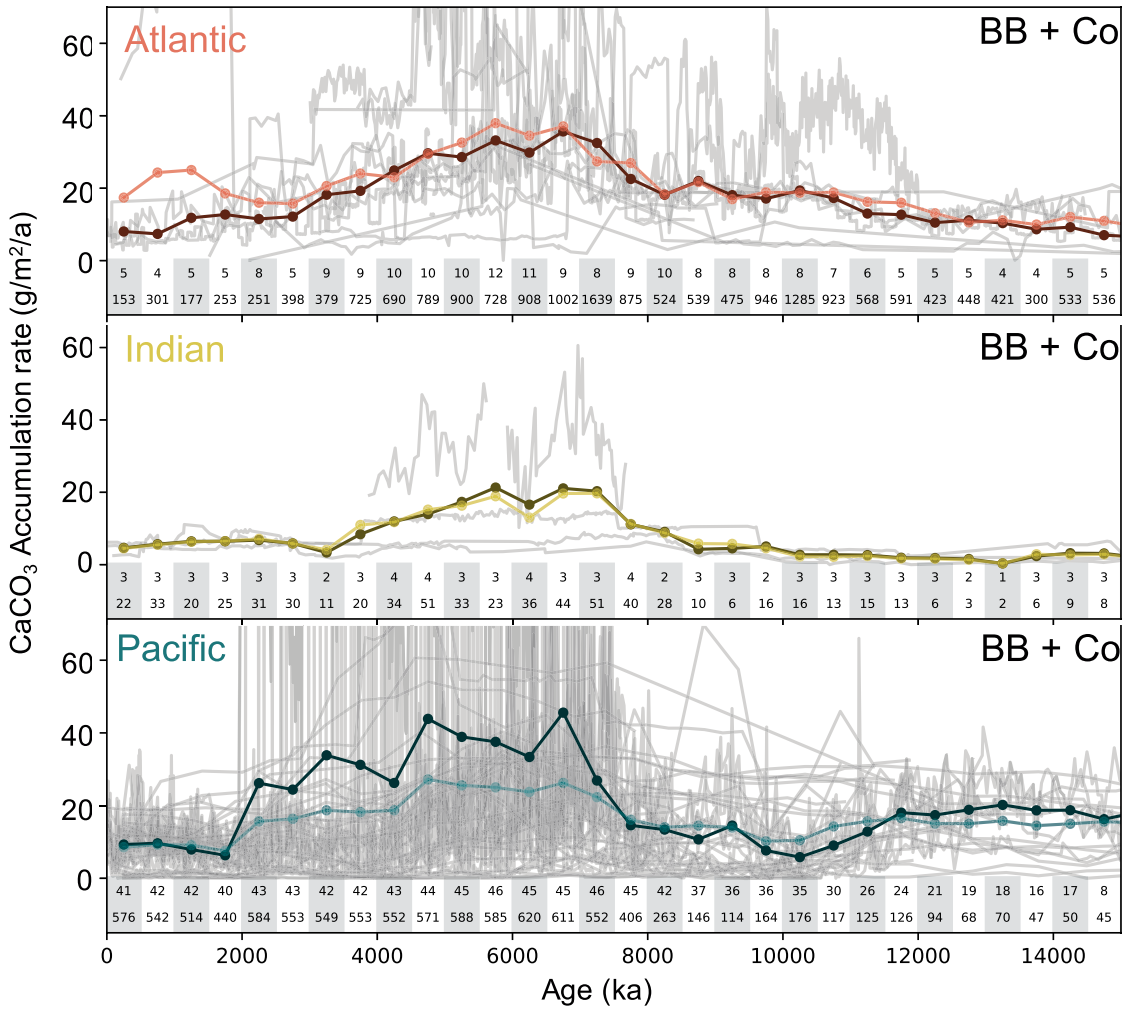

Figure 4. $CaCO_3$ accumulation rate from "BB" and "Co" labeled data sets for the three oceanic basins. Red, yellow, and blue lines represent "same weight" average (light color) and "resolution weight" average (dark color), respectively, for each basin. The light gray lines represent the raw data used to calculate the average. Below each graph, we show the number of data sets used to calculate the average for each 500 kyr time bin (top line), and the number of data averaged (bottom line). The same figure with only the "BB" labeled sites can be found in Figure S1 in Supporting Information S1. The standard deviations and outliers are shown in Figure S2 in Supporting Information S1. The averaged values for the three basins and the standard deviations are available in Table S2.

3.3. Temporal Analysis of the Compilation

We also looked at the synchronicity of the event between different oceanic basins using time series that we computed following the procedure described in Section 2 (Figure 4). The values indicated hereafter are those of the "resolution weight" average of the data sets (meaning that data sets with better resolution have a higher weighting in the average). This average was chosen because it gives a stronger signal. However, the signals obtained with the two averages have the same trends. The $CaCO_3$ accumulation rate was chosen because this variable is present in many data sets and has often been used to label data sets as "BB" or "Co." In the Atlantic Ocean, the signal was constructed from 12 different data sets labeled "BB" or "Co," with a maximum of 1,639 data and a minimum of 153 in one bin. On this time series, $CaCO_3$ accumulation rate increases since 15 ± 0.25 Ma with a strong increase around 7.5 ± 0.25 Ma (+15.3 $g/m^2/y$). The maximum is reached around 7 ± 0.25 Ma (34.1 $g/m^2/y$) and then there is a decrease that starts around 6.5 ± 0.25 Ma and ends around 2 ± 0.25 Ma. In the Indian Ocean, the signal was constructed from four different data sets labeled "BB" or "Co," with a maximum of 51 data and a minimum of 2 in a bin. There is an increase around 7.5 ± 0.25 Ma (+10 $g/m^2/y$) with a maximum around 7 ± 0.25 Ma (20.5 $g/m^2/y$) than a decrease around 5.5 ± 0.25 Ma. In the Pacific Ocean, the signal was constructed from 46 data sets labeled "BB" or "Co," with a maximum of 620 data and a minimum of 45 in one bin. There is an increase in the rate of $CaCO_3$ accumulation from 10 ± 0.25 Ma with a more abrupt increase

around 7.5 ± 0.25 Ma (+31.4 g/m^2/y). The maximum is around 7 ± 0.25 Ma (44.5 g/m^2/y) with a decrease until 2 ± 0.25 Ma. The comparison shows that the phase of increasing $CaCO_3$ accumulation rate around 7.5 ± 0.25 Ma is synchronous between the three oceanic basins. The synchronicity of the end of the event is less distinct, with the decrease in biogenic sediment accumulation being more abrupt in the Pacific Ocean than in the Atlantic and Indian Oceans. The time series with just data sets labeled "BB" follow the same trends (Figure S1 in Supporting Information S1).

4. Discussion

4.1. Compilation Biases and Limitations

Several biases need to be highlighted to evaluate the limitations of this compilation before discussing its contribution to the mechanistic understanding of the LMBB. To label the data sets, it was necessary to establish criteria that defined the LMBB. These criteria—described in Section 2—are based on the literature but are not necessarily shared by all authors, which makes it difficult to quantitatively and unequivocally identify the LMBB. Early studies defined the event in a specific region depending on local parameters and a bias may come from applying this definition globally. Indeed, the compilation showed that there was significant heterogeneity between data sets, which making a "global" definition difficult to apply. Observational biases are also present because the labeling of data sets relied on manual classification, as an automatic evaluation would have been too complicated due to the definition bias exposed previously. The "Co" label was created for this purpose.

An important bias may come from the sampling of the data compilation. Indeed, a non-negligible proportion of the data sets comes from studies focusing specifically on the LMBB, which therefore published data where the LMBB signature was visible. This potential bias toward record showing a clear LMBB signal, likely artificially decreases the number of data set without the LMBB signature. The DSDP program contains mostly sites with "No" labeled data sets, but the ODP program contains sites with data sets that are quite well distributed among the labels. The IODP program does not contain any sites with "No" labeled data sets (Figure 3c). Regarding dissolution effects, it is possible that depth plays a role in the presence or absence of the LMBB signature in the records. Although there seems to be no effect of depth on a global scale (Figure 3f), this could be the case locally. For example, for sites on the Walvis Ridge, ODP site 208-1264 (labeled "BB") is much shallower than ODP sites 208-1262, 208-1265, and 208-1266 (labeled "No"). Dissolution bias at global scale is however difficult to evaluate due to the carbonate compensation depth (CCD), which varied geographically (being different among basins, Berger & Winterer, 1975) and temporally (Dutkiewicz & Müller, 2022). In addition, the spatial distribution of sites included in the compilation is very heterogeneous. The majority of the compilation constitutes sites located in the Pacific Ocean (65%), while only 26% of the sites are located in the Atlantic Ocean and 9% in the Indian Ocean (Figure 2c). Very few sites are located at high latitudes (3.4% above 50°N and 2.5% below 50°S), or in the gyres of the South and North Pacific and of the North Atlantic oceans. This results in a geographically biased view of the LMBB as we lack information on the large-scale extension of the event. There is also temporal heterogeneity, as not all data sets cover exactly the same time interval. Many of them do indeed not cover the entire LMBB time interval. This heterogeneity may prevent a proper temporal analysis of the compilation (Figure 3b). Finally, some data sets come from studies with an orbital resolution and astronomical timescale (Drury et al., 2021), while others have only a few data points for a time window of several millions of years (Lyle, 2003). However, this resolution heterogeneity does not seem to impact labeling (Figure 3a): sites with an identified LMBB do not have a better resolution than the sites without an LMBB signature. These potential biases must be kept in mind when interpreting the data compilation.

Regarding the temporal interpretation of the compilation, it is important to consider that on the 500 kyr bins, there is an uncertainty of ±250 kyr, which is significant for the evaluation of timing relative to other events.

4.2. Does the Compilation Provide Support for Any of the LMBB Hypotheses Proposed in the Literature?

Despite the potential biases discussed above, our compilation has a worldwide coverage which opens the discussion on the origin of the LMBB. The compilation shows that the LMBB is globally distributed but is not expressed at all sites. Two hypotheses have been suggested in the literature to explain the existence of the event: (a) a global increase in the supply of nutrients to ocean basins through changes in continental weathering (Filippelli, 1997) and/or (b) a major redistribution of nutrients in the oceans (Farrell et al., 1995).

The spatial heterogeneity of the LMBB in the data compilation could be an element that supports the scenario of a change in nutrient supply from the continents. If this hypothesis is correct, the LMBB signal should be visible at some sites (close to nutrient input from the continents) and not at others (isolated from these inputs) or at least, its impact should be reduced with the increased distance from the source and without a specific local to regional effect of transfer from oceanic currents or winds. However, the compilation of data also showed the global nature of this event and a "local" cause such as the Himalayan uplift cannot produce a rise in productivity on a global scale without redistribution, or if it did, it would have been homogeneous for areas at a great distance from the source (i.e., in the Atlantic Ocean). Furthermore, sites in the data compilation that are located in the South China Sea (ODP sites 184-1143 and 184-1146), thus directly affected by the East Asian monsoon system, do not show a clear LMBB signal. Calculations of the distances of the sites from the nearest paleocoastline show that the LMBB is not present in areas particularly close to the coastline compared to areas where the LMBB appears to be absent, which partly contradicts this scenario. Nevertheless, it is important to consider that there can be local changes in the location of inputs that affect a particular site. For example, proximity of river outlet that changes its flow over time or shifting rainfall patterns. There is also evidence of micronutrient supply by dust fluxes which, due to wind, can be transported a long distance from their source (Diester-Haass et al., 2006; Hovan, 1995). This wind-driven dust supply is particularly important as it is related to the cooling and aridification of the late Miocene (Herbert et al., 2016; Pound et al., 2012). However, our data compilation cannot highlight an increase in dust flux during this time interval. Moreover, the nutrient input would be then restricted to areas downwind of the arid and desert regions which is not clearly the case in our records. Karatsolis et al. (2022) suggest an end of the LMBB at 4.6–4.4 Ma related to a decrease in insolation which in turn would have caused a reduction in hydrological cycle intensity and continental weathering. Our compilation shows a significant decline in carbonate-related productivity in the Pacific Ocean at this time, although it does not appear to correspond to the end of the LMBB. Moreover, there is no decline observed at this time in the Indian and Atlantic Oceans. Furthermore, the hypothesis of a particular orbital configuration as a trigger for the end of the LMBB is incompatible with our results because we show a slow and continuous decline of carbonate accumulation in the terminal part of the LMBB. This slow decrease started as soon as the maximum was reached, around 7–6.5 $\pm$ 0.25 Ma.

Regarding the nutrient redistribution hypothesis, the Eastern Equatorial Pacific is an interesting case study as it has been widely discussed in the LMBB literature (Farrell et al., 1995; Lyle et al., 2019; Reghellin et al., 2022). Our compilation shows that sites with an LMBB signature cluster between 6°N and 5°S and between 90°W and 127°W (Figure 5). The LMBB signature is present at eight sites (plus three controversial ones) and is absent at DSDP site 85-572. A closer look at the data for DSDP site 85-572 shows that there is a decrease in productivity from 10 Ma and then an increase from 5 Ma to a peak at 3.5 Ma. This site has not been labeled "BB" because instead of having an increase in productivity at the end of the Miocene, there is a decrease and the peak is reached at the moment when the "LMBB period" is over. The presence of this site without an LMBB might either be due to an error (in the definition of the event or in the interpretation of the signal) or to a particular geographical reason that remains undetermined. Without considering DSDP site 85-572, we observe that the sites where the LMBB is present were much closer to the Equator 10 Ma ago, which suggests an influence of equatorial upwelling on the increase in productivity (Lyle et al., 2019). Reghellin et al. (2022) suggested that the equatorial upwelling band was less parallel to the equator during the event and had a reduced spatial extent. Moreover, upwelling in this area appears to be strongest between 6.5 and 4.5 Ma, based on alkenone analyses from ODP sites 130-806 and 138-850 (Y. G. Zhang et al., 2017). These observations, which are in agreement with the compilation, support the scenario of nutrient redistribution as a driver of the LMBB. This redistribution may be a consequence of the closure of the Central American Seaway, which would result in the intensification of upwelling in the Eastern Equatorial Pacific, strongly increasing the surface nutrient concentration and thus primary productivity (Schneider & Schmittner, 2006). The Southeast Atlantic Ocean (around 30°S and 10°E) has also been studied in the context of the LMBB (Diester-Haass et al., 2004; Drury et al., 2021). In this area, the link between the LMBB and upwelling is more difficult to discern. Generally, sites, where the LMBB is present, are areas where simulated paleoproductivity is high (>0.5 g/cm^2/day; Figure 5) with the exception of ODP site 208-1264 (which is nonetheless the site with the highest resolution), which is in an area of low productivity (<0.4 g/cm^2/day) closely surrounded by five sites with no LMBB recorded. Sites without the LMBB are generally in areas of low simulated paleoproductivity with the exception of ODP site 75-530 and DSDP site 40-362 (for these sites, the hypothesis of redistribution remains open to discussion). The calculation of simulated palaeoproductivity for each site (Figure 3d) shows that on average, the LMBB signature is mostly recorded at sites located in areas of high productivity (e.g., upwelling areas). This is consistent with a scenario of intensification of ocean

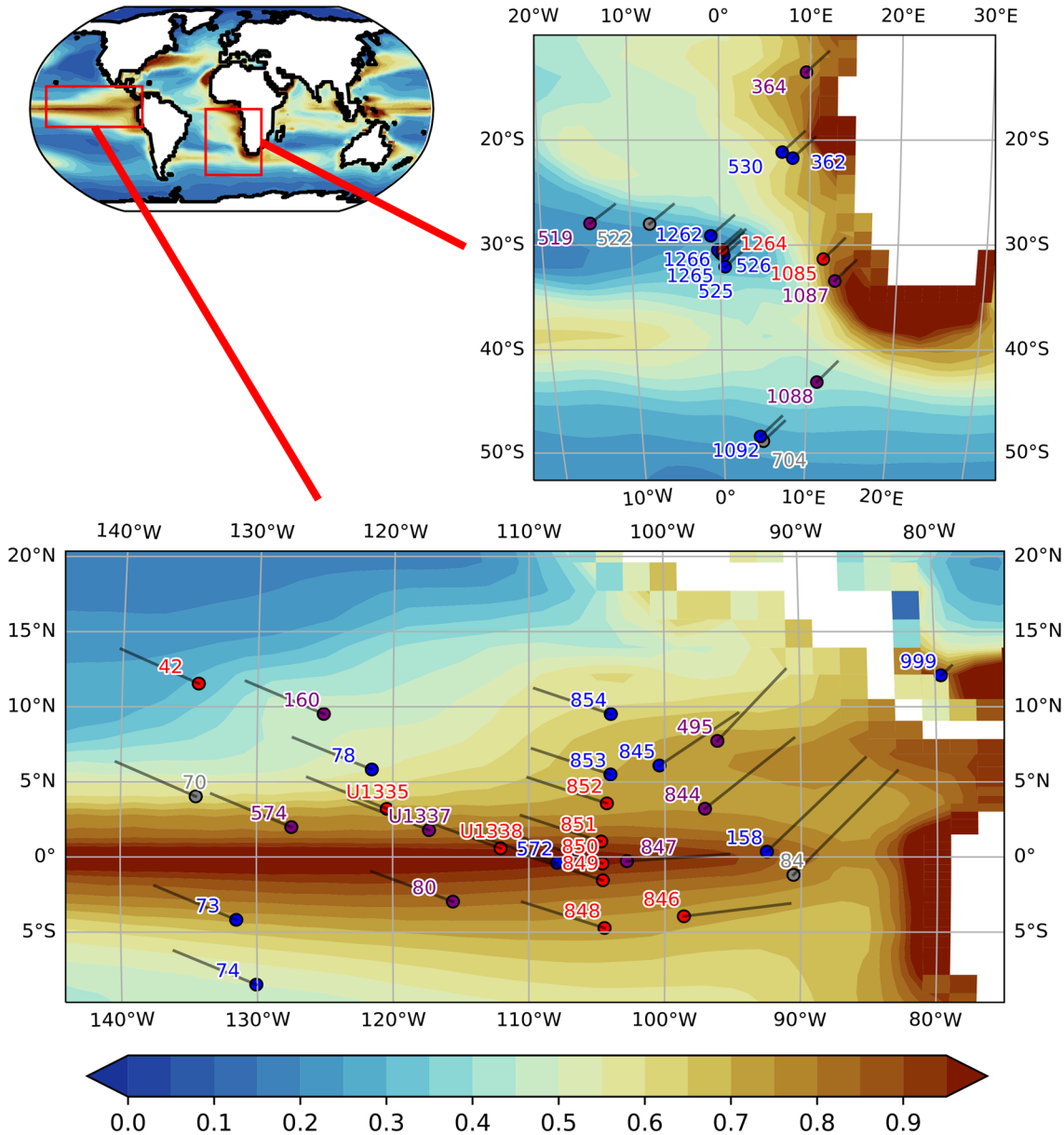

Figure 5. Integrated primary productivity by phytoplankton in g/m^2/day for the late Miocene (simulation output is from Sarr et al., 2022) with dots showing the paleo-positions (10 Ma) of the labeled sites. The black line at the end of each point indicates the present-day position of the site. A global figure can be found in Figure S3 in Supporting Information S1. Gray—Inconclusive; Blue—No LMBB; Purple—Controversial LMBB; and Red—LMBB is present.

circulation which can change the intensity of upwelling and induce a change in the vertical distribution of nutrients (Diester-Haass et al., 2002). Nutrient redistribution means that a transfer of nutrients from some geographic regions toward others (Dickens & Owen, 1996). This would be consistent with the heterogeneous nature of LMBB in the data compilation. But according to this model, some sites should show a decline in productivity. However, if there was an increase in overall nutrient input, it could mask this decline. Considering the low influence of depth on carbonate accumulation rates compiled here (Figure 3h), the fact that no productivity decreases are observed in the data compilation argues against the nutrient redistribution hypothesis.

An alternative scenario would be to consider an increase in nutrients on a global scale without (a) a redistribution (with an increase of productivity in some regions compensated by a decrease elsewhere) and (b) increase in continental inputs. This increase in nutrients could come from the generalized intensification of upwelling systems. This intensification could have two origins, an intensification of the wind regime or an increase in

deep water formation at high latitudes. The end of the Miocene is marked by a significant global cooling due to a decrease in the CO_2 level and a strengthening of the temperature gradient between the equator and the poles (Herbert et al., 2016; Martinot et al., 2022). The strengthening of this gradient leads to more air mass movement in the atmosphere and thus to an intensification of the Walker and Hadley cells (Kamae et al., 2011). Trade wind intensification is one consequence of this atmospheric reorganization, evidence of which has been observed in marine sediments (Hovan, 1995). The intensification of trade winds causes an increase in upwelling by Ekman pumping, especially in the equatorial Pacific (Bjerknes, 1969; Shankle et al., 2021) and results in increased productivity (Diester-Haass et al., 2006; Y. G. Zhang et al., 2017; Huguet et al., 2022). The late Miocene is also a period when the thermohaline circulation dominated by NADW and Antarctic Bottom Water became perennial (Poore et al., 2006). In general, NADW formation is thought to have intensified from the Miocene to the present day but its evolution is difficult to quantify (Poore et al., 2006). There are many factors that could have increased NADW production/strength in the late Miocene. For example, the decrease in CO_2 levels (Rae et al., 2021) in the late Miocene may have intensified NADW production (Bradshaw et al., 2015) as well as the transition from a mid-Miocene to present-day geography (Herold et al., 2012). NADW may also be enhanced by the closure of the Central America Seaway (Nisancioglu et al., 2003; Schneider & Schmittner, 2006; Sepulchre et al., 2014), thought to have occurred during the Miocene (Montes et al., 2015). Bierman et al. (2016) showed that a small ice sheet might have existed on Greenland over the past 7.5 Ma. An ice sheet on Greenland can lead to an intensification of NADW, through atmospheric forcing (Pillot et al., 2022). Finally, NADW production also varied with the depth of the Greenland Scotland Ridge, which had phases of uplift and subsidence in the late Miocene (Hossain et al., 2020; Poore et al., 2006; Wright & Miller, 1996). Increased deep water formation results in the intensification of overturning cells (such as the AMOC) and therefore intensified upwelling systems. Kiel et al. (2023) observe a large negative excursion in neodymium isotope values (from shark tooth enamel in southern Peru) around 8–7 Ma, which they attribute to the northward spread of Antarctic intermediate waters causing increased upwelling in this region. Following the same logic, a decrease in NADW production could have caused the end of the LMBB. The opening of the Bering Seaway in the early Pliocene (Gladenkov & Gladenkov, 2004), which according to modeling work could have caused a weakening of the AMOC (Brierley & Fedorov, 2016), could potentially have been linked to the end of the LMBB. The mechanisms put forward in this last hypothesis are not incompatible with the mechanisms of the other two hypotheses discussed in the previous paragraphs.

4.3. Speculation on the Link Between the Beginning of the LMBB and the Late Miocene Carbon Isotope Shift

The new data compilation confirms that there is a synchronicity between the onset of the LMBB and the Late Miocene Carbon Isotope Shift (LMCIS) (Drury et al., 2017; Keigwin, 1979; Westerhold et al., 2020) for the three oceanic basins, a synchronicity that has already been discussed in the literature (Dickens & Owen, 1999; Diester-Haass et al., 2005; Grant & Dickens, 2002). This approximately 1‰ negative shift in benthic foraminiferal $\delta^{13}C$ extends from 7.5 to 6.7 Ma and corresponds to the last major carbon cycle perturbation in Earth's history (Steinthorsdottir et al., 2021). The period of the $\delta^{13}C$ shift (7.5–6.7 Ma) corresponds to the most important phase of increasing productivity in the compilation and the productivity maximum (approx. 500 kyr; Figure 6). However, the isotopic shift lasts less than 1 million year and $\delta^{13}C$ never returns to its initial state, whereas the LMBB lasts several million years and biogenic sediment accumulation returns to a pre-event state. The causes of the LMCIS shift are still poorly understood. It may result from a global shift in $\delta^{13}C_{DIC}$ (Bickert et al., 2004; Hodell et al., 2001) caused by fractionation of organic matter in surface waters (Bickert et al., 2004) or a change in continental carbon flux (Du et al., 2022). This change may have been caused by the rapid expansion of C_4 plants between 8 and 6 Ma (Cerling et al., 1997), although this hypothesis appears to be temporally inconsistent (Drury et al., 2017; Tauxe & Feakins, 2020). The LMCIS may also have originated from a global high productivity event in the surface ocean (Diester-Haass et al., 2005; Grant & Dickens, 2002). The link between the LMBB and LMCIS supposes that the input of nutrients from the continents would produce a peak in dissolution and therefore a decrease in $\delta^{13}C$ values of dissolved inorganic carbon (Berger, 1981; Bickert et al., 2004; Diester-Haass et al., 2005), yet this hypothesis is not consistent with our compilation, which shows no dissolution event. The LMCIS could also be a consequence of a change in global ocean circulation, in particular the contribution of NADW, which would result in a greater difference in $\delta^{13}C$ between deep waters from the north and those from the south (Butzin et al., 2011; Crichton et al., 2021; Hodell & Venz-Curtis, 2006; Poore et al., 2006; Thomas & Via, 2007). Considering the timing of the LMCIS (7.5–6.7 Ma), this hypothesis would support the NADW

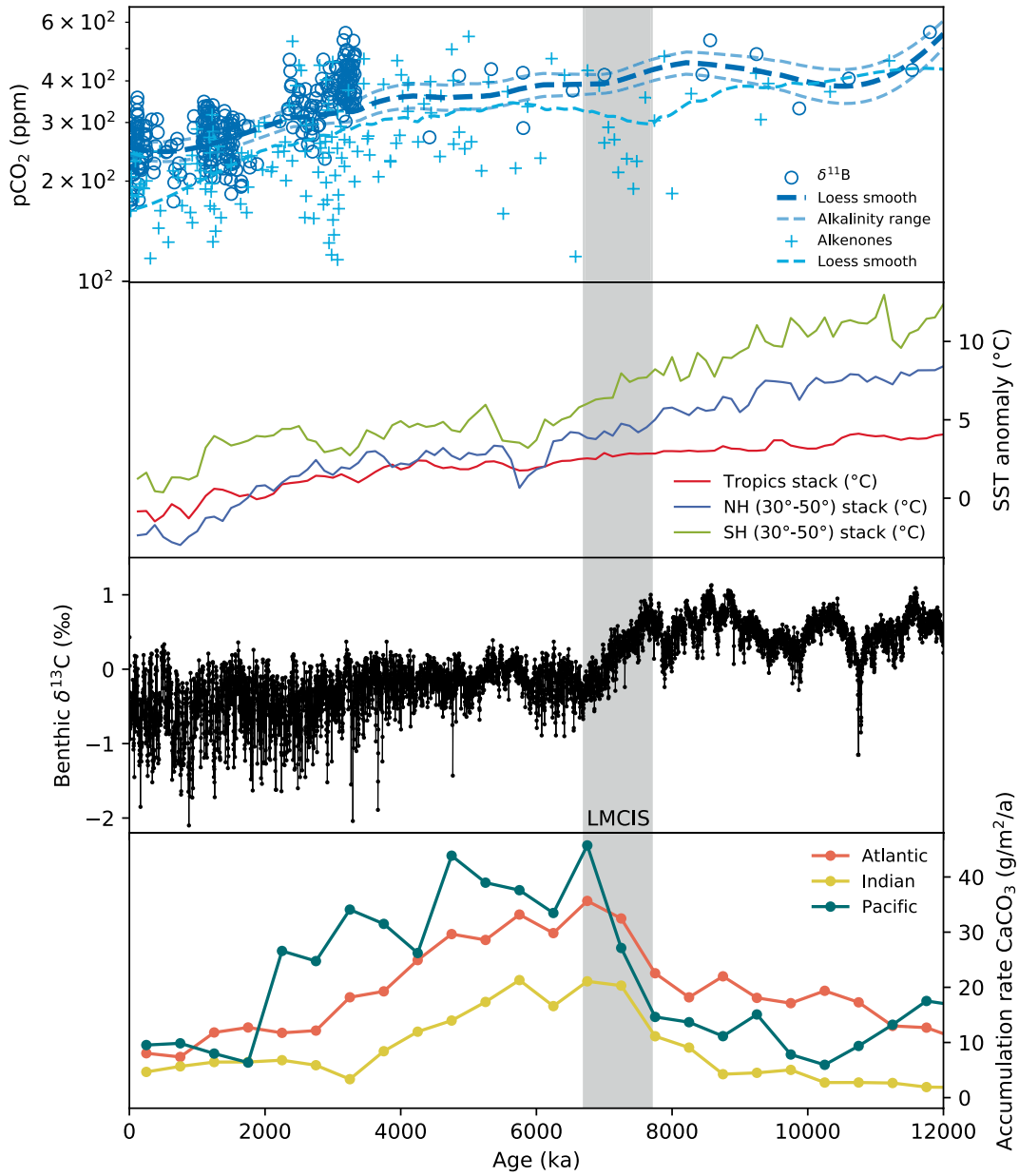

Figure 6. Top to bottom: Atmospheric pCO_2 reconstructions (ppm) from boron isotopes and alkenone $\delta^{13}C$ compiled in Rae et al. (2021). SST anomaly stacks for different latitudinal bands from Herbert et al. (2016). Megasplice benthic $\delta^{13}C$ evolution (‰) from Westerhold et al. (2020). $CaCO_3$ accumulation rate from "BB" and "Co" labeled data sets for the three ocean basins (Figure 4).

intensification scenario for the origin of the LMBB. In this case, the LMCIS would not be a consequence of the LMBB but a parallel consequence of a common cause.

5. Conclusion

Our data compilation confirms that expressions of the LMBB are present at many different locations but in a very heterogeneous way. We also show that the LMBB signature is absent from many sites. The compilation also shows that for the three oceanic basins, productivity strongly increases around 7.5 ± 0.25 Ma, peaks around 7 ± 0.25 Ma and then decreases until it reaches a pre-event state around 3.5 ± 0.25 Ma. To explain the origin of the LMBB, the scenarios of increased nutrient input to the oceans and a redistribution of nutrients in the

ocean cannot be ignored, although some aspects of our findings do not support these hypotheses. However, the compilation shows that the sites where the LMBB is recorded are mainly located in areas where there is a high productivity regime (i.e., upwelling systems). We propose that the most likely hypothesis to explain the onset and peak of the LMBB is a global increase in upwelling intensity due to an increase in wind strength or an increase in deep water formation, ramping up global ocean circulation. These increases may have been the result of major tectonic or climatic changes at the end of the Miocene, such as the restriction of the Central American Seaway, the general decrease in temperature and CO_2 levels, subsidence of the Greenland-Scotland Ridge or the establishment of the Greenland ice sheet. In future work, the forcing factors at the origin of the LMBB could be identified using a set of simulations from a coupled ocean/atmosphere model with late Miocene paleogeography and integrating a marine biogeochemistry module.

Data Availability Statement

All data used in this study have been previously published. However, because of the reevaluation of age-depth models, all data sets as used in this study have been deposited on SEANOE (Pillot, 2023). The metadata and the original citations are available for each data set in Table S1 and on SEANOE (Pillot, 2023). The time series of all variables in all data sets are also available in this repository.

Acknowledgments
The authors are grateful to the associate editor and the two anonymous reviewers for their relevant comments and suggestions that clearly improved the manuscript. The authors thank Johan Renaudie for his help in using Neptune Sandbox Berlin. The authors also thank Weimin Si for access to data and Jean-Baptiste Landant for discussions. This research was funded by the French ANR project MioCarb awarded to BSM (ANR-20-CE49-0002).

References

Aumont, O., Ethé, C., Tagliabue, A., Bopp, L., & Gehlen, M. (2015). PISCES-v2: An ocean biogeochemical model for carbon and ecosystem studies. *Geoscientific Model Development*, *8*(8), 2465–2513. https://gmd.copernicus.org/articles/8/2465/2015/

Berger, H. V. E. (1981). *Chemostratigraphy and biostratigraphic correlation: Exercises in systematic stratigraphy*. Oceanologica Acta. Retrieved from https://archimer.ifremer.fr/doc/00246/35689/

Berger, W. H., Leckie, R. M., Janecek, T. R., Stax, R., & Takayama, T. (1993). Neogene carbonate sedimentation on Ontong Java Plateau: Highlights and open questions. *Proceedings of the Ocean Drilling Program: Scientific Results*, *130*, 711–744. Retrieved from http://www-odp.tamu.edu/publications/130_SR/130TOC.HTM

Berger, W. H., & Winterer, E. L. (1975). Plate stratigraphy and the fluctuating carbonate line. In *Pelagic sediments: On land and under the sea* (pp. 11–48). John Wiley & Sons, Ltd. Retrieved from https://onlinelibrary.wiley.com/doi/abs/10.1002/9781444304855.ch2

Berggren, W. A., Kent, D. V., Aubry, M.-P., & Hardenbol, J. (1995). Geochronology, time scales and global stratigraphic correlation.

Berggren, W. A., Kent, D. V., Flynn, J. J., & Van Couvering, J. A. (1985). Cenozoic geochronology. *Geological Society of America Bulletin*, *96*(11), 1407. Retrieved from https://pubs.geoscienceworld.org/gsabulletin/article/96/11/1407-1418/202998

Bickert, T., Haug, G. H., & Tiedemann, R. (2004). Late Neogene benthic stable isotope record of Ocean Drilling Program Site 999: Implications for Caribbean paleoceanography, organic carbon burial, and the Messinian Salinity Crisis. *Paleoceanography*, *19*(1), PA1023. https://doi.org/10.1029/2002PA000799

Bierman, P. R., Shakun, J. D., Corbett, L. B., Zimmerman, S. R., & Rood, D. H. (2016). A persistent and dynamic East Greenland Ice Sheet over the past 7.5 million years. *Nature*, *540*(7632), 256–260. https://doi.org/10.1038/nature20147

Bjerknes, J. (1969). Atmospheric teleconnections from the equatorial Pacific. *Monthly Weather Review*, *97*(3), 163–172. https://doi.org/10.1175/1520-0493(1969)097⟨0163:ATFTEP⟩2.3.CO;2

Bolton, C. T., Gray, E., Kuhnt, W., Holbourn, A. E., Lübbers, J., Grant, K., et al. (2022). Secular and orbital-scale variability of equatorial Indian Ocean summer monsoon winds during the late Miocene. *Climate of the Past*, *18*(4), 713–738. Retrieved from https://cp.copernicus.org/articles/18/713/2022/

Bradshaw, C. D., Lunt, D. J., Flecker, R., & Davies-Barnard, T. (2015). Disentangling the roles of late Miocene palaeogeography and vegetation – Implications for climate sensitivity. *Palaeogeography, Palaeoclimatology, Palaeoecology*, *417*, 17–34. https://doi.org/10.1016/j.palaeo.2014.10.003

Breza, J. (1992). High-resolution study of neogene ice-rafted debris, site 751, southern Kerguelen plateau (p. 120). https://doi.org/10.2973/odp.proc.sr.120.1992

Brierley, C. M., & Fedorov, A. V. (2016). Comparing the impacts of Miocene–Pliocene changes in inter-ocean gateways on climate: Central American Seaway, Bering Strait, and Indonesia. *Earth and Planetary Science Letters*, *444*, 116–130. Retrieved from https://linkinghub.elsevier.com/retrieve/pii/S0012821X16300978

Butzin, M., Lohmann, G., & Bickert, T. (2011). Miocene ocean circulation inferred from marine carbon cycle modeling combined with benthic isotope records. *Paleoceanography*, *26*(1), PA1203. https://doi.org/10.1029/2009PA001901

Cao, X., Zahirovic, S., Li, S., Suo, Y., Wang, P., Liu, J., & Müller, R. D. (2022). A deforming plate tectonic model of the South China Block since the Jurassic. *Gondwana Research*, *102*, 3–16. Retrieved from https://linkinghub.elsevier.com/retrieve/pii/S1342937X20303051

Cerling, T. E., Harris, J. M., MacFadden, B. J., Leakey, M. G., Quade, J., Eisenmann, V., & Ehleringer, J. R. (1997). Global vegetation change through the Miocene/Pliocene boundary. *Nature*, *389*(6647), 153–158. Retrieved from http://www.nature.com/articles/38229

Clift, P. D., Kulhanek, D. K., Zhou, P., Bowen, M. G., Vincent, S. M., Lyle, M., & Hahn, A. (2020). Chemical weathering and erosion responses to changing monsoon climate in the late miocene of southwest Asia. *Geological Magazine*, *157*(6), 939–955. https://doi.org/10.1017/s0016756819000608

Cook, C. P., van de Flierdt, T., Williams, T., Hemming, S. R., Iwai, M., Kobayashi, M., et al. (2013). Dynamic behaviour of the East Antarctic ice sheet during Pliocene warmth. *Nature Geoscience*, *6*(9), 765–769. Retrieved from https://www.nature.com/articles/ngeo1889

Cortese, G., Gersonde, R., Hillenbrand, C.-D., & Kuhn, G. (2004). Opal sedimentation shifts in the World Ocean over the last 15 Myr. *Earth and Planetary Science Letters*, *224*(3–4), 509–527. https://doi.org/10.1016/j.epsl.2004.05.035

Crichton, K. A., Ridgwell, A., Lunt, D. J., Farnsworth, A., & Pearson, P. N. (2021). Data-constrained assessment of ocean circulation changes since the middle Miocene in an Earth system model. *Climate of the Past*, *17*(5), 2223–2254. Retrieved from https://cp.copernicus.org/articles/17/2223/2021/

Crocker, A. J., Naafs, B. D. A., Westerhold, T., James, R. H., Cooper, M. J., Röhl, U., et al. (2022). Astronomically controlled aridity in the Sahara since at least 11 million years ago. *Nature Geoscience*, *15*(8), 671–676. https://doi.org/10.1038/s41561-022-00990-7

Curry, W., Shackleton, N., Richter, C., Backman, J., Bassinot, F., Bickert, T., et al. (1995). *Leg synthesis. Proceedings Ocean Drilling Program*, Initial Reports 155 (pp. 17–21). Ocean Drilling Program.

Dickens, G. R., & Owen, R. M. (1996). Sediment geochemical evidence for an early-middle Gilbert (early Pliocene) productivity peak in the North Pacific Red Clay Province. *Marine Micropaleontology*, *27*(1–4), 107–120. https://doi.org/10.1016/0377-8398(95)00054-2

Dickens, G. R., & Owen, R. M. (1999). The latest Miocene–Early Pliocene biogenic bloom: A revised Indian Ocean perspective. *Marine Geology*, *161*(1), 75–91. https://doi.org/10.1016/S0025-3227(99)00057-2

Diester-Haass, L., Billups, K., & Emeis, K. C. (2005). In search of the late Miocene–early Pliocene "biogenic bloom" in the Atlantic Ocean (Ocean Drilling Program Sites 982, 925, and 1088). *Paleoceanography*, *20*(4), PA4001. https://doi.org/10.1029/2005PA001139

Diester-Haass, L., Billups, K., & Emeis, K. C. (2006). Late Miocene carbon isotope records and marine biological productivity: Was there a (dusty) link? *Paleoceanography*, *21*(4), PA4216. https://doi.org/10.1029/2006PA001267

Diester-Haass, L., Meyers, P. A., & Bickert, T. (2004). Carbonate crash and biogenic bloom in the late Miocene: Evidence from ODP Sites 1085, 1086, and 1087 in the Cape Basin, southeast Atlantic Ocean. *Paleoceanography*, *19*(1), PA1007. https://doi.org/10.1029/2003PA000933

Diester-Haass, L., Meyers, P. A., & Vidal, L. (2002). The late Miocene onset of high productivity in the Benguela Current upwelling system as part of a global pattern. *Marine Geology*, *180*(1–4), 87–103. https://doi.org/10.1016/S0025-3227(01)00207-9

Dobson, D. M., Dickens, G. R., & Rea, D. K. (2001). Terrigenous sediment on Ceara Rise: A Cenozoic record of South American orogeny and erosion. *Palaeogeography, Palaeoclimatology, Palaeoecology*, *165*(3–4), 215–229. https://doi.org/10.1016/S0031-0182(00)00161-9

Drury, A. J., Liebrand, D., Westerhold, T., Beddow, H. M., Hodell, D. A., Rohlfs, N., et al. (2021). Climate, cryosphere and carbon cycle controls on Southeast Atlantic orbital-scale carbonate deposition since the Oligocene (30–0 Ma). *Climate of the Past*, *17*(5), 2091–2117. https://doi.org/10.5194/cp-17-2091-2021

Drury, A. J., Westerhold, T., Frederichs, T., Tian, J., Wilkens, R., Channell, J. E., et al. (2017). Late Miocene climate and time scale reconciliation: Accurate orbital calibration from a deep-sea perspective. *Earth and Planetary Science Letters*, *475*, 254–266. https://doi.org/10.1016/j.epsl.2017.07.038

Du, J., Tian, J., & Ma, W. (2022). The Late Miocene Carbon Isotope Shift driven by synergetic terrestrial processes: A box-model study. *Earth and Planetary Science Letters*, *584*, 117457. https://doi.org/10.1016/j.epsl.2022.117457

Dutkiewicz, A., & Müller, R. D. (2021). The carbonate compensation depth in the South Atlantic Ocean since the Late Cretaceous. *Geology*, *49*(7), 873–878. https://doi.org/10.1130/G48404.1

Dutkiewicz, A., & Müller, R. D. (2022). The history of Cenozoic carbonate flux in the Atlantic Ocean constrained by multiple regional carbonate compensation depth reconstructions. *Geochemistry, Geophysics, Geosystems*, *23*(11), e2022GC010667. https://doi.org/10.1029/2022GC010667

Farrell, J. W., & Janecek, T. R. (1991). Late Neogene paleoceanography and paleoclimatology of the northeast Indian Ocean (site 758) (p. 121). https://doi.org/10.2973/odp.proc.sr.121.1991

Farrell, J. W., Raffi, I., Janecek, T. R., Murray, D. W., Levitan, M., Dadey, K. A., et al. (1995). Late Neogene sedimentation patterns in the eastern equatorial Pacific Ocean (p. 40).

Filippelli, G. M. (1997). Intensification of the Asian monsoon and a chemical weathering event in the late Miocene–early Pliocene: Implications for late Neogene climate change (Vol. *4*).

Gardner, J. V., Dean, W. E., Bisagno, L., Hemphill, E., & Survey, U. G. (1986). Late neogene and quaternary coarse-fraction and carbonate stratigraphies for site 586 on Ontong-Java plateau and site 591 on Lord Howe Rise (Vol. *90*). https://doi.org/10.2973/dsdp.proc.90.1986

Gladenkov, A. Y., & Gladenkov, Y. B. (2004). Onset of connections between the Pacific and Arctic Oceans through the Bering Strait in the Neogene. *Stratigraphy and Geological Correlation*, *12*(2), 13.

Gradstein, F. M., Ogg, J. G., Schmitz, M. D., Ogg, G. M., Agterberg, F. P., Anthonissen, D. E., et al. (2012). *The geologic time scale* In F. M. Gradstein, J. G. Ogg, M. D. Schmitz, & G. M. Ogg (Eds.), (pp. ix–xi). Elsevier. https://doi.org/10.1016/B978-0-444-59425-9.10003-4

Gradstein, F. M., Ogg, J. G., Schmitz, M. D., Ogg, G. M., Agterberg, F. P., Aretz, M., et al. (2020). In F. M. Gradstein, J. G. Ogg, M. D. Schmitz, & G. M. Ogg (Eds.), *Geologic time scale 2020* (pp. xi–xiv). Elsevier. https://doi.org/10.1016/B978-0-12-824360-2.00036-X

Gradstein, F. M., Ogg, J. G., & Smith, A. G. (2004). *A geologic time scale 2004* (p. 589). Cambridge Universtiy Press.

Grant, K. M., & Dickens, G. R. (2002). Coupled productivity and carbon isotope records in the southwest Pacific Ocean during the late miocene–early pliocene biogenic bloom. *Palaeogeography, Palaeoclimatology, Palaeoecology*, *187*(1–2), 61–82. https://doi.org/10.1016/s0031-0182(02)00508-4

Gupta, A. K., Singh, R. K., Joseph, S., & Thomas, E. (2004). Indian Ocean high-productivity event (10–8 Ma): Linked to global cooling or to the initiation of the Indian monsoons? *Geology*, *32*(9), 753. https://doi.org/10.1130/G20662.1

Hayward, B. W., Johnson, K., Sabaa, A. T., Kawagata, S., & Thomas, E. (2010). Cenozoic record of elongate, cylindrical, deep-sea benthic foraminifera in the North Atlantic and equatorial Pacific Oceans. *Marine Micropaleontology*, *74*(3–4), 75–95. https://doi.org/10.1016/j.marmicro.2010.01.001

Helland, P., & Holmes, M. (1997). Surface textural analysis of quartz sand grains from ODP Site 918 off the southeast coast of Greenland suggests glaciation of southern Greenland at 11 Ma. *Palaeogeography, Palaeoclimatology, Palaeoecology*, *135*(1–4), 109–121. https://doi.org/10.1016/S0031-0182(97)00025-4

Herbert, T. D., Lawrence, K. T., Tzanova, A., Peterson, L. C., Caballero-Gill, R., & Kelly, C. S. (2016). Late Miocene global cooling and the rise of modern ecosystems. *Nature Geoscience*, *9*(11), 843–847. https://doi.org/10.1038/ngeo2813

Hermoyian, C. S., & Owen, R. M. (2001). Late Miocene-early Pliocene biogenic bloom: Evidence from low-productivity regions of the Indian and Atlantic Oceans. *Paleoceanography*, *16*(1), 95–100. https://doi.org/10.1029/2000PA000501

Herold, N., Huber, M., Müller, R. D., & Seton, M. (2012). Modeling the Miocene climatic optimum: Ocean circulation. *Paleoceanography*, *27*(1), PA1209. https://doi.org/10.1029/2010PA002041

Hodell, D. A., Curtis, J. H., Sierro, F. J., & Raymo, M. E. (2001). Correlation of Late Miocene to Early Pliocene sequences between the Mediterranean and North Atlantic. *Paleoceanography*, *16*(2), 164–178. https://doi.org/10.1029/1999PA000487

Hodell, D. A., & Venz-Curtis, K. A. (2006). Late Neogene history of deepwater ventilation in the Southern Ocean. *Geochemistry, Geophysics, Geosystems*, *7*(9), Q09001. https://doi.org/10.1029/2005GC001211

Holbourn, A. E., Kuhnt, W., Clemens, S. C., Kochhann, K. G. D., Jöhnck, J., Lübbers, J., & Andersen, N. (2018). Late Miocene climate cooling and intensification of southeast Asian winter monsoon. *Nature Communications*, *9*(1), 1584. https://doi.org/10.1038/s41467-018-03950-1

Hossain, A., Knorr, G., Lohmann, G., Stärz, M., & Jokat, W. (2020). Simulated thermohaline fingerprints in response to different Greenland-Scotland Ridge and Fram Strait subsidence histories. *Paleoceanography and Paleoclimatology*, *35*(7), e2019PA003842. https://doi.org/10.1029/2019PA003842

Hovan, S. A. (1995). 28. Late Cenozoic atmospheric circulation intensity and climatic history recorded by Eolian deposition in the Eastern Equatorial Pacific Ocean, Leg 138. *Proceedings of the Ocean Drilling Program, Scientific Results*, 615–625.

Huguet, C., Jaeschke, A., & Rethemeyer, J. (2022). Paleoclimatic and palaeoceanographic changes coupled to the Panama Isthmus closing (13–4Ma) using organic proxies (p. 40).

Janecek, T. R. (1985). Eolian sedimentation in the northwest Pacific Ocean: A preliminary examination of the data from Deep Sea Drilling project sites 576 and 578 (p. 86). https://doi.org/10.2973/dsdp.proc.86.1985

John, S., & Krissek, L. A. (2002). The late Miocene to Pleistocene ice-rafting history of southeast Greenland (Vol. *8*).

Kamae, Y., Ueda, H., & Kitoh, A. (2011). Hadley and Walker circulations in the Mid-Pliocene Warm period simulated by an atmospheric general circulation model. *Journal of the Meteorological Society of Japan. Series II*, *89*(5), 475–493. https://doi.org/10.2151/jmsj.2011-505

Karatsolis, B. T., Lougheed, B. C., De Vleeschouwer, D., & Henderiks, J. (2022). Abrupt conclusion of the late Miocene-early Pliocene biogenic bloom at 4.6-4.4 Ma. *Nature Communications*, *13*(1), 353. https://doi.org/10.1038/s41467-021-27784-6

Keigwin, L. D. (1979). Late Cenozoic stable isotope stratigraphy and paleoceanography of DSDP sites from the East Equatorial and Central North Pacific ocean (p. 22).

Kiel, S., Jakubowicz, M., Altamirano, A., Belka, Z., Dopieralska, J., Urbina, M., & Salas-Gismondi, R. (2023). The late Cenozoic evolution of the Humboldt Current System in coastal Peru: Insights from neodymium isotopes. *Gondwana Research*, *116*, 104–112. https://doi.org/10.1016/j.gr.2022.12.008

Kuhnt, W., Holbourn, A., Hall, R., Zuvela, M., & Käse, R. (2004). Neogene history of the Indonesian throughflow. In *Continent-ocean interactions within East Asian marginal seas* (pp. 299–320). American Geophysical Union. https://doi.org/10.1029/149GM16

Lübbers, J., Kuhnt, W., Holbourn, A., Bolton, C., Gray, E., Usui, Y., et al. (2019). The Middle to Late Miocene "carbonate crash" in the Equatorial Indian Ocean. *Paleoceanography and Paleoclimatology*, *34*(5), 813–832. https://doi.org/10.1029/2018PA003482

Lyle, M. (2003). Neogene carbonate burial in the Pacific Ocean. *Paleoceanography*, *18*(3), 1059. https://doi.org/10.1029/2002PA000777

Lyle, M., & Baldauf, J. (2015). Biogenic sediment regimes in the Neogene equatorial Pacific, IODP Site U1338: Burial, production, and diatom community. *Palaeogeography, Palaeoclimatology, Palaeoecology*, *433*, 106–128. https://doi.org/10.1016/j.palaeo.2015.04.001

Lyle, M., Dadey, K. A., & Farrel, J. W. (1995). The late miocene (11-8 ma) eastern pacific carbonate crash: Evidence for reorganization of deep-water circulation by the closure of the Panama gateway (Vol. *138*). https://doi.org/10.2973/odp.proc.sr.138.1995

Lyle, M., Drury, A. J., Tian, J., Wilkens, R., & Westerhold, T. (2019). Late Miocene to Holocene high-resolution eastern equatorial Pacific carbonate records: Stratigraphy linked by dissolution and paleoproductivity. *Climate of the Past*, *15*(5), 1715–1739. https://doi.org/10.5194/cp-15-1715-2019

Martinot, C., Bolton, C. T., Sarr, A.-C., Donnadieu, Y., Garcia, M., Gray, E., & Tachikawa, K. (2022). Drivers of late Miocene tropical sea surface cooling: A new perspective from the equatorial Indian Ocean (accepted). *Paleoceanography and Paleoclimatology*, *37*, e2021PA004407. https://doi.org/10.1002/essoar.10509655.2

Montes, C., Cardona, A., Jaramillo, C., Pardo, A., Silva, J. C., Valencia, V., et al. (2015). Middle Miocene closure of the Central American Seaway. *Science*, *348*(6231), 226–229. https://doi.org/10.1126/science.aaa2815

Müller, D. W., Hodell, D. A., & Ciesielski, P. F. (1991). Late Miocene to earliest Pliocene (9.8-4.5 ma) paleoceanography of the subantarctic Southeast Atlantic: Stable isotopic, sedimentologic, and microfossil evidence (Vol. *114*). https://doi.org/10.2973/odp.proc.sr.114.1991

Müller, R. D., Zahirovic, S., Williams, S. E., Cannon, J., Seton, M., Bower, D. J., et al. (2019). A global plate model including lithospheric deformation along major rifts and orogens since the triassic. *Tectonics*, *38*(6), 1884–1907. https://doi.org/10.1029/2018TC005462

Nisancioglu, K. H., Raymo, M. E., & Stone, P. H. (2003). Reorganization of Miocene deep water circulation in response to the shoaling of the Central American Seaway. *Paleoceanography*, *18*(1), 1006. https://doi.org/10.1029/2002PA000767

O'Dea, A., Lessios, H. A., Coates, A. G., Eytan, R. I., Restrepo-Moreno, S. A., Cione, A. L., et al. (2016). Formation of the Isthmus of Panama. *Science Advances*, *2*(8), e1600883. https://doi.org/10.1126/sciadv.1600883

Pälike, H., Lyle, M. W., Nishi, H., Raffi, I., Ridgwell, A., Gamage, K., et al. (2012). A Cenozoic record of the equatorial Pacific carbonate compensation depth. *Nature*, *488*(7413), 609–614. https://doi.org/10.1038/nature11360

Palike, H., Norris, R. D., Herrle, J. O., Wilson, P. A., Coxall, H. K., Lear, C. H., et al. (2006). The heartbeat of the Oligocene climate system. *Science*, *314*(5807), 1894–1898. https://doi.org/10.1126/science.1133822

Peterson, L., & Backman, J. (1990). Late cenozoic carbonate accumulation and the history of the carbonate compensation depth in the western equatorial Indian Ocean (pp. 467–507).

Pillot, Q. (2023). Compilation of published data from oceanic drilling that covers the late Miocene and early Pliocene interval for the study of the Late Miocene Biogenic Bloom [Dataset]. SEANOE. Retrieved from https://www.seanoe.org/data/00820/93168/

Pillot, Q., Donnadieu, Y., Sarr, A.-C., Ladant, J.-B., & Suchéras-Marx, B. (2022). Evolution of ocean circulation in the North Atlantic Ocean during the Miocene: Impact of the Greenland Ice Sheet and the Eastern Tethys Seaway. *Paleoceanography and Paleoclimatology*, *37*(8), e2022PA004415. https://doi.org/10.1029/2022PA004415

Pisias, N., Mayer, L., Janecek, T., Palmer-Julson, A., & van Andel, T. (Eds.), (1995). *Proceedings of the Ocean Drilling Program, 138 Scientific Results* (Vol. 138). Ocean Drilling Program. https://doi.org/10.2973/odp.proc.sr.138.1995

Poore, H. R., Samworth, R., White, N. J., Jones, S. M., & McCave, I. N. (2006). Neogene overflow of northern component water at the Greenland-Scotland Ridge. *Geochemistry, Geophysics, Geosystems*, *7*(6), Q06010. https://doi.org/10.1029/2005GC001085

Pound, M. J., Haywood, A. M., Salzmann, U., & Riding, J. B. (2012). Global vegetation dynamics and latitudinal temperature gradients during the Mid to Late Miocene (15.97–5.33Ma). *Earth-Science Reviews*, *112*(1–2), 1–22. https://doi.org/10.1016/j.earscirev.2012.02.005

Qin, X., Müller, R. D., Cannon, J., Landgrebe, T. C. W., Heine, C., Watson, R. J., & Turner, M. (2012). The GPlates geological information model and markup language. *Geoscientific Instrumentation, Methods and Data Systems*, *1*(2), 111–134. https://doi.org/10.5194/gi-1-111-2012

Rae, J. W., Zhang, Y. G., Liu, X., Foster, G. L., Stoll, H. M., & Whiteford, R. D. (2021). Atmospheric CO2 over the past 66 million years from marine archives. *Annual Review of Earth and Planetary Sciences*, *49*(1), 609–641. https://doi.org/10.1146/annurev-earth-082420-063026

Reghellin, D., Coxall, H. K., Dickens, G. R., Galeotti, S., & Backman, J. (2022). The Late Miocene-Early Pliocene biogenic bloom in the eastern equatorial pacific: New Insights from Integrated Ocean Drilling Program Site U1335. *Paleoceanography and Paleoclimatology*, *37*(3), e2021PA004313. https://doi.org/10.1029/2021PA004313

Renaudie, J. (2019). NSBcompanion. *Zenodo*. Retrieved from https://zenodo.org/record/3408198

Renaudie, J., Lazarus, D., & Diver, P. (2020). NSB (Neptune Sandbox Berlin): An expanded and improved database of marine planktonic microfossil data and deep-sea stratigraphy. *Palaeontologia Electronica*, *23*(1), a11. Retrieved from https://palaeo-electronica.org/content/2020/2966-the-nsb-database

Sarr, A.-C., Donnadieu, Y., Bolton, C. T., Ladant, J.-B., Licht, A., Fluteau, F., et al. (2022). Neogene South Asian monsoon rainfall and wind histories diverged due to topographic effects. *Nature Geoscience*, *15*(4), 314–319. https://doi.org/10.1038/s41561-022-00919-0

Schneider, B., & Schmittner, A. (2006). Simulating the impact of the Panamanian seaway closure on ocean circulation, marine productivity and nutrient cycling. *Earth and Planetary Science Letters*, *246*(3–4), 367–380. https://doi.org/10.1016/j.epsl.2006.04.028

Schuster, M., Duringer, P., Ghienne, J.-F., Vignaud, P., Mackaye, H. T., Likius, A., & Brunet, M. (2006). The age of the Sahara desert. *Science*, *311*(5762), 821. https://doi.org/10.1126/science.1120161

Sepulchre, P., Arsouze, T., Donnadieu, Y., Dutay, J.-C., Jaramillo, C., Le Bras, J., et al. (2014). Consequences of shoaling of the Central American Seaway determined from modeling Nd isotopes. *Paleoceanography*, *29*(3), 176–189. https://doi.org/10.1002/2013PA002501

Sepulchre, P., Caubel, A., Ladant, J.-B., Bopp, L., Boucher, O., Braconnot, P., et al. (2020). IPSL-CM5A2 – An Earth system model designed for multi-millennial climate simulations. *Geoscientific Model Development*, *13*(7), 3011–3053. https://doi.org/10.5194/gmd-13-3011-2020

Shankle, M. G., Burls, N. J., Fedorov, A. V., Thomas, M. D., Liu, W., Penman, D. E., et al. (2021). Pliocene decoupling of equatorial Pacific temperature and pH gradients. *Nature*, *598*(7881), 457–461. https://doi.org/10.1038/s41586-021-03884-7

Si, W., & Rosenthal, Y. (2019). Reduced continental weathering and marine calcification linked to late Neogene decline in atmospheric CO2. *Nature Geoscience*, *12*(10), 833–838. https://doi.org/10.1038/s41561-019-0450-3

Stax, R., & Stein, R. (1993). Long-term changes in the accumulation of organic carbon in Neogene sediments, Ontong Java Plateau (Vol. *130*). https://doi.org/10.2973/odp.proc.sr.130.1993

Steinthorsdottir, M., Coxall, H. K., de Boer, A. M., Huber, M., Barbolini, N., Bradshaw, C. D., et al. (2021). The Miocene: The future of the past. *Paleoceanography and Paleoclimatology*, *36*(4), e2020PA004037. https://doi.org/10.1029/2020PA004037

Tauxe, L., & Feakins, S. J. (2020). A reassessment of the chronostratigraphy of Late Miocene C3–C4 transitions. *Paleoceanography and Paleoclimatology*, *35*(7), e2020PA003857. https://doi.org/10.1029/2020PA003857

Thomas, D. J., & Via, R. K. (2007). Neogene evolution of Atlantic thermohaline circulation: Perspective from Walvis Ridge, southeastern Atlantic Ocean. *Paleoceanography*, *22*(2), PA2212. https://doi.org/10.1029/2006PA001297

Torsvik, T. H., Steinberger, B., Shephard, G. E., Doubrovine, P. V., Gaina, C., Domeier, M., et al. (2019). Pacific-Panthalassic reconstructions: Overview, errata and the way forward. *Geochemistry, Geophysics, Geosystems*, *20*(7), 3659–3689. https://doi.org/10.1029/2019GC008402

Wagner, T. (2002). Late cretaceous to early quaternary organic sedimentation in the eastern Equatorial Atlantic. *Palaeogeography, Palaeoclimatology, Palaeoecology*, *179*(1–2), 113–147. https://doi.org/10.1016/S0031-0182(01)00415-1

Wang, C., Dai, J., Zhao, X., Li, Y., Graham, S. A., He, D., et al. (2014). Outward-growth of the Tibetan Plateau during the Cenozoic: A review. *Tectonophysics*, *621*, 1–43. https://doi.org/10.1016/j.tecto.2014.01.036

Wang, R., Li, J., & Li, B. (2004). *Data report: Late miocene–quaternary biogenic opal accumulation at ODP site 1143* (Vol. 12). Southern South China Sea.

Westerhold, T., Marwan, N., Drury, A. J., Liebrand, D., Agnini, C., Anagnostou, E., et al. (2020). An astronomically dated record of Earth's climate and its predictability over the last 66 million years. *Science*, *369*(6509), 1383–1387. https://doi.org/10.1126/science.aba6853

Winkler, A. (1999). GEOMAR Forschungszentrum fA˜ ¼marine Geowissenschaften WischhofstraA˜Y 1-3, 24148 Kiel, Bundesrepublik Deutschland (p. 130).

Wright, J. D., & Miller, K. G. (1996). Control of North Atlantic Deep Water circulation by the Greenland-Scotland Ridge. *Paleoceanography*, *11*(2), 157–170. https://doi.org/10.1029/95PA03696

Yang, R., Yang, Y., Fang, X., Ruan, X., Galy, A., Ye, C., et al. (2019). Late Miocene intensified tectonic uplift and climatic aridification on the Northeastern Tibetan Plateau: Evidence from clay mineralogical and geochemical records in the Xining Basin. *Geochemistry, Geophysics, Geosystems*, *20*(2), 829–851. https://doi.org/10.1029/2018GC007917

Young, A., Flament, N., Maloney, K., Williams, S., Matthews, K., Zahirovic, S., & Müller, R. D. (2019). Global kinematics of tectonic plates and subduction zones since the late Paleozoic Era. *Geoscience Frontiers*, *10*(3), 989–1013. https://doi.org/10.1016/j.gsf.2018.05.011

Zhang, L., Chen, M., Xiang, R., Zhang, L., & Lu, J. (2009). Productivity and continental denudation history from the South China Sea since the late Miocene. *Marine Micropaleontology*, *72*(1–2), 76–85. https://doi.org/10.1016/j.marmicro.2009.03.006

Zhang, Y. G., Pagani, M., Henderiks, J., & Ren, H. (2017). A long history of equatorial deep-water upwelling in the Pacific Ocean. *Earth and Planetary Science Letters*, *467*, 1–9. https://doi.org/10.1016/j.epsl.2017.03.016

Zhang, Z., Ramstein, G., Schuster, M., Li, C., Contoux, C., & Yan, Q. (2014). Aridification of the Sahara desert caused by Tethys Sea shrinkage during the Late Miocene. *Nature*, *513*(7518), 401–404. https://doi.org/10.1038/nature13705